Origin of Transient and Intermittent Dynamics in Spatiotemporal Chaotic Systems

Erico L. Rempel*

Institute of Aeronautical Technology (ITA) and World Institute for Space Environment Research (WISER), CTA/ITA/IEFM, São José dos Campos-SP, 12228-900, Brazil

Abraham C.-L. Chian

National Institute for Space Research (INPE) and World Institute for Space Environment Research (WISER), P.O. Box 515, São José dos Campos-SP, 12227-010, Brazil

(Received 31 March 2006; published 2 January 2007)

Nonattracting chaotic sets (chaotic saddles) are shown to be responsible for transient and intermittent dynamics in an extended system exemplified by a nonlinear regularized long-wave equation, relevant to plasma and fluid studies. As the driver amplitude is increased, the system undergoes a transition from quasiperiodicity to temporal chaos, then to spatiotemporal chaos. The resulting intermittent time series of spatiotemporal chaos displays random switching between laminar and bursty phases. We identify temporally and spatiotemporally chaotic saddles which are responsible for the laminar and bursty phases, respectively. Prior to the transition to spatiotemporal chaos, a spatiotemporally chaotic saddle is responsible for chaotic transients that mimic the dynamics of the post-transition attractor.

DOI: 10.1103/PhysRevLett.98.014101 PACS numbers: 05.45.Jn, 47.27.Cn, 47.27.ed

Spatiotemporal chaos (STC) refers to the state where a spatially extended system is chaotic in time and irregular in space. Several works have tried to identify the mechanisms for transition to STC. As one varies a control parameter (e.g., Reynolds number, Re), at some critical value the spatially homogeneous steady state becomes unstable with respect to small perturbations, giving rise to periodic oscillations. For increasing Re, secondary and higher order instabilities lead to symmetry breaking of spatiotemporal patterns, resulting in states that are disordered in space and time [1]. Depending on the system, this sequence of instabilities can lead to diverse dynamical phenomena such as phase chaos, characterized by the absence of defects [2], and defect chaos or Bloch-front turbulence, where localized structures undergo nucleation and annihilation due to instabilities of periodic patterns or fronts [3]. Apart from the aforementioned transitions to STC, a number of works have reported sequences of bifurcations that evolve to STC via quasiperiodicity, and/or temporal chaos in numerical simulations [4–7] and laboratory experiments [8].

A spatiotemporal chaotic behavior can reflect asymptotic chaos when it is governed by an attracting chaotic set, or transient chaos when it is governed by nonattracting chaotic sets known as chaotic saddles [9]. In this Letter we explore the role of chaotic attractors and chaotic saddles in transition to temporal and spatiotemporal chaos in a nonlinear regularized long-wave equation with applications to wave dynamics in fluids and plasmas. The study of chaotic transients has shed light onto the understanding of transition to turbulence in numerical simulations of plane Couette and pipe flows [10], where it is suggested that the turbulent state corresponds to a chaotic saddle.

In addition to chaotic transients, another important topic in spatiotemporal chaotic systems is intermittency. Intermittent spatiotemporal series displays random alternations of qualitatively different behaviors, and recent works have proposed some possible explanations for its origins in turbulent flows [11]. From the point of view of dynamical systems, a series of papers [12–15] has revealed the crucial role of chaotic saddles in the generation of intermittent dynamics after chaotic transitions such as interior and merging crises. The resulting intermittent time series displays alternate switching between different chaotic saddles embedded in the postcrisis attractor. The same behavior has been observed in systems described by maps [12], ordinary [13], and partial differential equations [14,15]. In all those references, the chaotic attractors are of low dimension, with a fractal dimension smaller than 3 and the dynamics are chaotic in time but regular in space. As stated in Ref. [7], the mechanism for intermittency in spatially extended systems is still open.

In the present Letter it is shown that chaotic saddles are responsible for chaotic transients and intermittency in a high-dimensional extended system. After a transition to spatiotemporal chaos, the intermittent time series displays random switching between phases of temporal and spatiotemporal chaos. The two main contributions of this Letter are the following: (a) before the transition to spatiotemporal chaos we identify a spatiotemporally chaotic saddle responsible for chaotic transients that mimic the dynamics of the post-transition attractor and can be used to predict its behavior, and (b) after the transition to spatiotemporal chaos, we describe a procedure to identify temporally and spatiotemporally chaotic saddles responsible for the two phases of the intermittent regime. The presence of this scenario in other systems is discussed.

The driven-damped nonlinear regularized long-wave equation is given by [6,7]

$$\partial_t \phi + a\partial_{txx}\phi + c\partial_x \phi + f\phi\partial_x \phi = -\gamma\phi - \varepsilon \sin(x - \Omega t), \quad (1)$$

where we fix $a = -0.287$, $c = 1$, $f = -6$, $\gamma = 0.1$, and $\Omega = 0.65$, following Refs. [6,7]. Thus, the only control parameter is the driver amplitude ε. Equation (1) can be used to study space-charge waves and drift waves in magnetized plasmas [6], as well as shallow water waves in fluids [16]. Periodic boundary conditions are considered, $\phi(x, t) = \phi(x + 2\pi, t)$, and Eq. (1) is solved with the pseudospectral method by assuming $\phi(x, t) = \sum_{k=-N}^{N} b_k(t)e^{ikx}$ and obtaining a set of ordinary differential equations for the complex Fourier coefficients $b_k(t)$. The following results are obtained with $N = 32$, since this number of modes is sufficient to reproduce the transition to spatiotemporal chaos reported in Refs. [6]. A Poincaré map is defined by $\mathrm{Re}[b_1(t)] = 0$ and $d\mathrm{Re}[b_1(t)]/dt > 0$.

Figure 1 shows the spatiotemporal evolution of ϕ for three values of ε. The pattern in Fig. 1(a), obtained for $\varepsilon = 0.191$, is spatially regular and quasiperiodic in time, with a maximum Lyapunov exponent $\lambda_{\max} = 0$. The origin of this quasiperiodic attractor (QPA) through a sequence of bifurcations of a limit cycle was studied in Ref. [7]. The spatiotemporal pattern in Fig. 1(b) at $\varepsilon = 0.199$ is very similar to the QPA of Fig. 1(a). However, a positive maximum Lyapunov exponent $\lambda_{\max} \approx 0.06$ reveals the chaotic nature of the attractor. Since the dynamics on this attractor is spatially coherent, we call it temporally chaotic attractor (TCA). The transition from QPA to TCA occurs at $\varepsilon \approx 0.1925$. Further increase in ε leads to the onset of spatiotemporal chaos via crisis after the collision of the temporal chaos (TC) attractor with an unstable saddle orbit at $\varepsilon_c \approx 0.1994$ [6]. Figure 1(c) depicts the spatiotemporally chaotic attractor (STCA) at $\varepsilon = 0.201$, where the maximum Lyapunov exponent suddenly jumps to $\lambda_{\max} \approx 1.83$. Figure 2(a) shows the convergence of $\lambda_{\max}$ for the chaotic attractors and chaotic saddles found at $\varepsilon = 0.199$ and $\varepsilon = 0.201$. The relation between both sets of exponents is discussed later in this Letter.

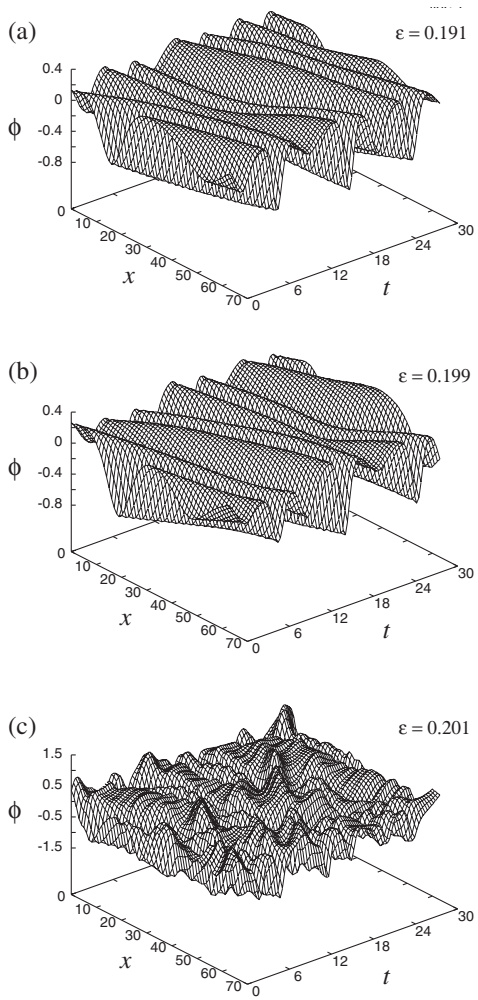

FIG. 1. Spatiotemporal evolution of ϕ for (a) $\varepsilon = 0.191$ (QPA); (b) $\varepsilon = 0.199$ (TCA) and (c) $\varepsilon = 0.201$ (STCA).

The change from TC to STC can also be measured by the correlation dimension [17]. Denote the N points of a long series of Poincaré points on the attractor by $\{\mathbf{X}_i\}_{i=1}^{N}$. The correlation function $C(r)$ is computed as $C(r) = \lim_{N\to\infty}(1/N^2)\sum_{i,j=1}^{N}\theta(r - |\mathbf{X}_i - \mathbf{X}_j|)$, where $\theta(x)$ is the Heaviside function. For sufficiently small values of r, $C(r)$ behaves as a power law of r. Figure 2(b) is a plot of $\log_2 C(r)$ versus $\log_2 r$ for the TC attractor ($\varepsilon = 0.199$, circles), and the STC attractor ($\varepsilon = 0.201$, triangles). The straight lines with slope β are obtained from a least squares fitting of the computed data, and give the correlation dimension of the attractors in the Poincaré map. The dimensions in the full phase space are ≈ 3.16 for the TC

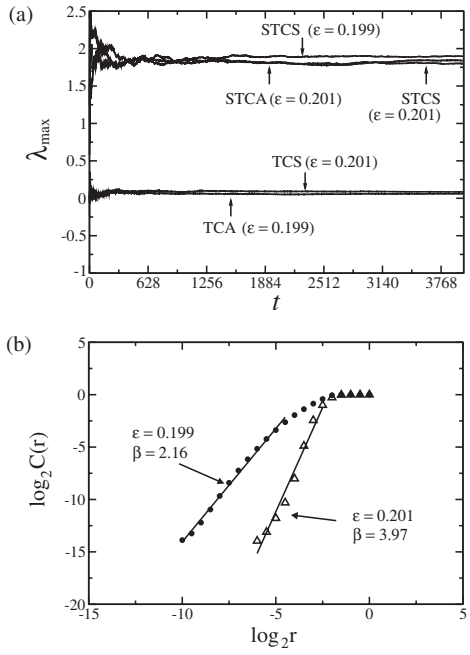

FIG. 2. (a) Maximum Lyapunov exponents $\lambda_{\max}$ for the chaotic attractors and chaotic saddles at $\varepsilon = 0.199$ and $\varepsilon = 0.201$. (b) Correlation dimension for the chaotic attractors TCA ($\varepsilon = 0.199$) and STCA ($\varepsilon = 0.201$) in the Poincaré map.

attractor and ≈ 4.97 for the STC attractor. This shows that the STC attractor is a high-dimensional chaotic set embedded in the 64-dimensional Fourier space.

Figure 3 shows time series of the "wave energy," $E(t) = \int_0^{2\pi}[\phi^2 - a\phi_x^2]dx/4\pi$. In Fig. 3(a), for $\varepsilon = 0.191$, after an initial transient of highly erratic large-amplitude fluctuations, the solution converges to the quasiperiodic attractor. A similar dynamics is seen in Fig. 3(b) for the TC attractor at $\varepsilon = 0.199$, where oscillations are more irregular than in the quasiperiodicity (QP) regime. For the STC attractor at $\varepsilon = 0.201$, the energy time series displays highly erratic large-amplitude oscillations, interspersed with phases of small-amplitude dynamics [Fig. 3(c)]. The high-amplitude "bursty" phases resemble the transient part of the time series in Figs. 3(a) and 3(b) and the low-amplitude "laminar" phases resemble the TC regime of Fig. 3(b).

An inspection of the Poincaré map is helpful at this point. Figure 4 shows the two-dimensional projections $\mathrm{Re}(b_2)$ vs $\mathrm{Re}(b_3)$ of numerically computed attractors and chaotic saddles. The QP attractor of Fig. 4(a) (black dots)

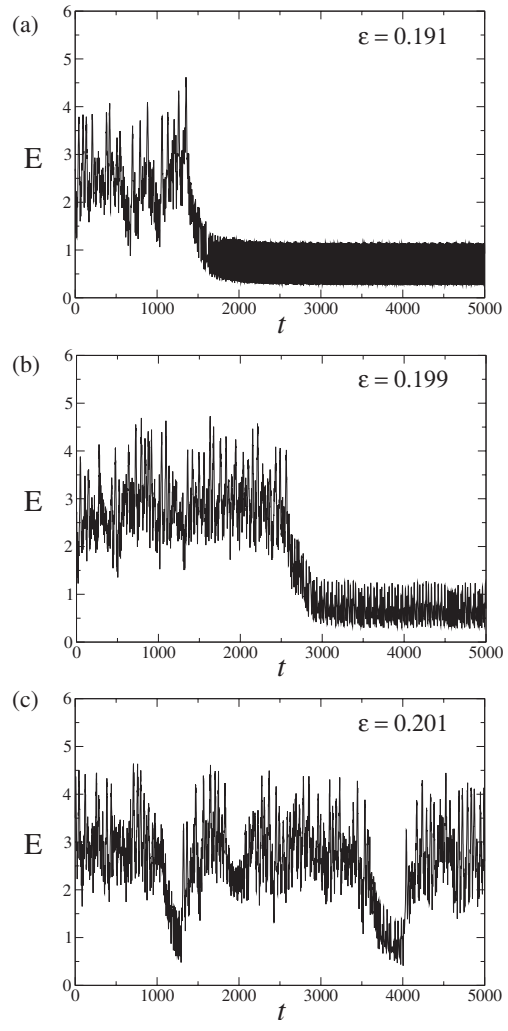

FIG. 3. Time series of the wave energy for (a) QPA at $\varepsilon = 0.191$; (b) TCA at $\varepsilon = 0.199$; (c) STCA at $\varepsilon = 0.201$.

corresponds to the intersection of a torus with the Poincaré section. In Fig. 4(b) the torus has been broken, but the trajectory on the TC attractor still wanders around the former torus. The surrounding STC saddle (gray dots) was found with the sprinkler method [14,18]. In the sprinkler method, the chaotic saddle is approximated by points from trajectories that follow long transients before escaping from a predefined restraining region of the phase space. To find the STC saddle, a large set of initial conditions is iterated and those trajectories for which $E(t) > 1.2$ for 100 consecutive iterations of the Poincaré map ($t \approx 1000$) are considered to be in the vicinity of the STC saddle. For each of those trajectories, the first 40 and last 40 iterations are discarded and only 20 points are plotted [18]. In both Figs. 4(a) and 4(b) the STC saddle is responsible for transient spatiotemporal chaos. Figure 4(c) depicts the STC attractor at $\varepsilon = 0.201$, and a comparison with Fig. 4(b) shows that the spatiotemporally chaotic saddle (STCS) is embedded in the STC attractor.

After the transition to spatiotemporal chaos, the TC attractor loses its asymptotic stability and trajectories can escape from it and gain access to the STC saddle embedded in STCA. By taking initial conditions on the region of the former TC attractor and applying the sprinkler method, one finds a second, smaller, temporally chaotic saddle embedded in the STC attractor. This TC saddle is responsible for the laminar phases of the intermittent time series, and is plotted in Fig. 4(d) (black dots) along with the STCS (gray dots). The dynamics of a typical trajectory on the STC attractor goes as follows. While in the vicinity of the TC saddle, the orbit follows the temporally chaotic and spatially coherent dynamics basically governed by the TC saddle. After a transient time, the trajectory escapes from this TC region and jumps to the surrounding region, where its dynamics is spatiotemporally chaotic and is basically governed by the STC saddle. This corresponds to the bursty phases of the intermittent time series. Again, after a transient time the trajectory is reinjected into the TC region and the process is repeated.

The relation between the attracting and nonattracting chaotic sets can be investigated by means of a comparison of their maximum Lyapunov exponents $\lambda_{\max}$ [see Fig. 2(a)]. The value of $\lambda_{\max}$ for TCA ($\lambda_{\max} \approx 0.06$) at $\varepsilon = 0.199$ is close to the value for the temporally chaotic saddle (TCS) ($\lambda_{\max} \approx 0.08$) at $\varepsilon = 0.201$, as expected. Also, $\lambda_{\max}$ varies only slightly for STCS at different parameter values, remaining very close to the value of $\lambda_{\max}$ for the STCA at $\varepsilon = 0.201$ ($\lambda_{\max} \approx 1.84$ for STCA and $\lambda_{\max} \approx 1.8$ for STCS). This happens because at $\varepsilon = 0.201$ the bursty phases dominate the dynamics of STCA, as seen in the time series of Fig. 3(c). Note that since $\lambda_{\max} \approx 1.89$ for STCS at $\varepsilon = 0.199$, the precrisis STCS can be used to predict the dynamics of the postcrisis attractor.

In summary, the transition from QP to TC, then to STC in a nonlinear regularized long-wave equation was studied using chaotic saddles as the building blocks. Before the transition to STC, the system is either quasiperiodic or

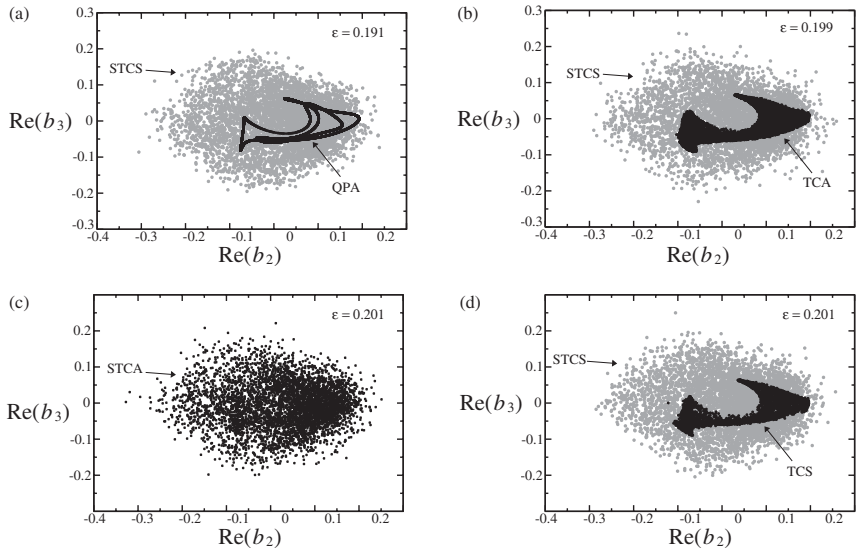

FIG. 4. (a) Spatiotemporally chaotic saddle (STCS, gray) and quasiperiodic attractor (QPA, black) at $\varepsilon = 0.191$; (b) STCS (gray) and temporally chaotic attractor (TCA, black) at $\varepsilon = 0.199$; (c) spatiotemporally chaotic attractor (STCA) at $\varepsilon = 0.201$; (d) STCS (gray) and temporally chaotic saddle (TCS, black) embedded in STCA at $\varepsilon = 0.201$.

chaotic in time but regular in space, whereby the wave energy is concentrated in a narrow k spectrum. At the onset of STC the spatial regularity is destroyed, analogous to the phenomenon of wave breaking, which leads to energy cascade due to nonlinear wave-wave interactions, resulting in a broad k spectrum and irregularity in space. A similar scenario has recently been observed in a transition to STC via QP-TC in an extended system described by the damped Kuramoto-Sivashinsky equation [19]. We suggest that this scenario can be readily found in extended dissipative dynamical systems that exhibit transient STC prior to the transition to sustained STC, which evolve from TC to STC via a crisislike chaotic transition, e.g., the pipe flow experiment [20], and nonlinear optical systems [21]. In fact, the QP-TC route to STC has been observed in a model of ring of cardiac cells [5] and several laboratory experiments of drift waves in plasmas [8], where the results of the present Letter can be applied.

This Letter is supported by CNPq and FAPESP.

*Electronic address: rempel@ita.br

[1] M. C. Cross and P. C. Hohenberg, Rev. Mod. Phys. **65**, 851 (1993); H. L. Swinney, in *Critical Problems in Physics*, edited by V. L. Fitch, D. R. Marlow, and M. A. E. Dementi (Princeton University Press, Princeton, 1997); T. Bohr *et al.*, *Dynamical Systems Approach to Turbulence* (Cambridge University Press, Cambridge, 1998).

[2] I. S. Aranson and L. Kramer, Rev. Mod. Phys. **74**, 99 (2002).

[3] J. Davidsen and R. Kapral, Phys. Rev. Lett. **91**, 058303 (2003); B. Marts, A. Hagberg, E. Meron, and A. L. Lin, *ibid.* **93**, 108305 (2004).

[4] S. Kida, M. Yamada, and K. Ohkitani, Lect. Notes Numer. Appl. Anal. **10**, 31 (1989); L. van Veen, Physica (Amsterdam) **210D**, 249 (2005).

[5] Zhilin Qu, J. N. Weiss, and A. Garfinkel, Phys. Rev. Lett. **78**, 1387 (1997).

[6] Kaifen He, Phys. Rev. Lett. **80**, 696 (1998); **84**, 3290 (2000); Phys. Rev. E **63**, 016218 (2000); Kaifen He and A. C.-L. Chian, Phys. Rev. Lett. **91**, 034102 (2003); Phys. Rev. E **69**, 026207 (2004).

[7] Kaifen He, Phys. Rev. Lett. **94**, 034101 (2005).

[8] J. H. Chu and I. Lin, Phys. Rev. A **39**, 233 (1989); T. Klinger *et al.*, Phys. Rev. Lett. **79**, 3913 (1997); F. Brochard, E. Gravier, and G. Bonhomme, Phys. Rev. E **73**, 036403 (2006).

[9] H. E. Nusse and J. A. Yorke, Physica (Amsterdam) **36D**, 137 (1989).

[10] B. Eckhardt and A. Mersmann, Phys. Rev. E **60**, 509 (1999); J. D. Skufca, J. A. Yorke, and B. Eckhardt, Phys. Rev. Lett. **96**, 174101 (2006).

[11] B. W. Zeff *et al.*, Nature (London) **421**, 146 (2003); Y. Li and C. Meneveau, Phys. Rev. Lett. **95**, 164502 (2005).

[12] K. G. Szabo, Y. C. Lai, T. Tel, and C. Grebogi, Phys. Rev. Lett. **77**, 3102 (1996); Phys. Rev. E **61**, 5019 (2000).

[13] E. L. Rempel and A. C.-L. Chian, Int. J. Bifurcation Chaos Appl. Sci. Eng. **14**, 4009 (2004); E. L. Rempel *et al.*, Physica (Amsterdam) **199D**, 407 (2004).

[14] E. L. Rempel and A. C.-L. Chian, Phys. Lett. A **319**, 104 (2003); E. L. Rempel *et al.*, Chaos **14**, 545 (2004).

[15] E. L. Rempel and A. C.-L. Chian, Phys. Rev. E **71**, 016203 (2005).

[16] T. B. Benjamin, J. L. Bona, and J. J. Mahony, Phil. Trans. R. Soc. A **272**, 47 (1972); M. A. Manna and V. Merle, Phys. Rev. E **57**, 6206 (1998); R. A. Kraenkel, M. A. Manna, and V. Merle, *ibid.* **60**, 2418 (1999).

[17] P. Grassberger and I. Procaccia, Phys. Rev. Lett. **50**, 346 (1983).

[18] H. Kantz and P. Grassberger, Physica (Amsterdam) **17D**, 75 (1985); G.-H. Hsu, E. Ott, and C. Grebogi, Phys. Lett. A **127**, 199 (1988).

[19] E. L. Rempel and A. C.-L. Chian (to be published).

[20] J. Peixinho and T. Mullin, Phys. Rev. Lett. **96**, 094501 (2006).

[21] M. Sauer and F. Kaiser, Int. J. Bifurcation Chaos Appl. Sci. Eng. **6**, 1481 (1996).